November 1, 1995

Laminar Natural Convection in a Discretely Heated Cavity: I—Assessment of Three-Dimensional Effects

Theodore J. Heindel, *Purdue University*
S. Ramadhyani, *Purdue University*
F. P. Incropera, *Purdue University*

Laminar Natural Convection in a Discretely Heated Cavity: I—Assessment of Three-Dimensional Effects

T. J. Heindel[1]

S. Ramadhyani

F. P. Incropera

Heat Transfer Laboratory,
School of Mechanical Engineering,
Purdue University,
West Lafayette, IN 47907-1288

Two and three-dimensional calculations have been performed for laminar natural convection induced by a 3 × 3 array of discrete heat sources flush-mounted to one vertical wall of a rectangular cavity whose opposite wall was isothermally cooled. Edge effects predicted by the three-dimensional model yielded local and average Nusselt numbers that exceeded those obtained from the two-dimensional model, as well as average surface temperatures that were smaller than the two-dimensional predictions. For heater aspect ratios $A_{htr} \lesssim 3$, average Nusselt numbers increased with decreasing A_{htr}. However, for $A_{htr} \gtrsim 3$, the two and three-dimensional predictions were within 5 percent of each other and results were approximately independent of A_{htr}. In a companion paper (Heindel et al., 1995a), predictions are compared with experimental results and heat transfer correlations are developed.

Introduction

Continued advances in integrated circuit technology have contributed to significant improvements in computer performance, with workstations and powerful desktop computers gaining increased market penetration. However, these improvements are placing an increased demand on associated cooling requirements. A passive cooling system, employing natural convection, eliminates fan or pump assemblies required with forced convection cooling schemes, thereby providing a noise and vibration-free means of thermal control. Such cooling options have been assessed by addressing natural convection in discretely heated cavities, and reviews are presented by Jaluria (1985), Incropera (1988), Peterson and Ortega (1990), and Bar-Cohen (1992, 1993). However, the majority of these studies focus on single or multiple strip heat sources ($L_x = D$) and neglect three-dimensional effects, which can be significant for small heat sources arranged in closely spaced arrays. This study addresses implications of the two-dimensional assumption by comparing predictions with those obtained from a three-dimensional numerical model.

One of the first numerical studies of three-dimensional natural convection considered one or two discrete heat sources flush-mounted to one vertical wall of a cavity for which the opposite wall was cooled (Kuhn and Oosthuizen, 1986). The effect of heater location on heat transfer was shown to be small if the heated elements were located at least two element heights from the top or bottom walls. Outside this range, heat transfer was strongly influenced by location. If the element was near the cavity ceiling, fluid motion was inhibited and heat transfer was dominated by conduction. In studying element size effects, the height of the discrete heat source was shown to be more important than its width, unless, of course, the element width was much smaller than the height. Three-dimensional flow increased local heat transfer near the heater edges, causing the average Nusselt number to exceed results obtained from corresponding two-dimensional predictions.

A three-dimensional numerical analysis was also performed by Wroblewski and Joshi (1992), who investigated transient natural convection within a square enclosure ($A_x = A_z = 1$) with a single, protruding heat source mounted on one vertical wall. Although symmetry was not enforced, to determine if an unsteady plume would arise from the heat source, symmetric flow and temperature fields were predicted. Wroblewski and Joshi (1994) subsequently considered the effects of heater geometry for a constant protrusion height. For a square heat source, two-dimensional calculations yielded a maximum heater temperature 2.8 times higher than that predicted from the three-dimensional model. If the heater aspect ratio ($A_{htr} = L_x/L_z$) was greater than 4.0, the two and three-dimensional predictions agreed to within 10 percent.

Polentini et al. (1993) performed an extensive experimental study for a 3 × 3 heater array flush-mounted on one wall of an enclosure, with the opposing wall isothermally cooled. Heat transfer was independent of the enclosure aspect ratio ($2.5 \leq A_z \leq 7.5$) but increased with increasing angle of inclination, where the cold plate was always oriented above the heat sources. The increased heat transfer was due to increased turbulent mixing within the enclosure and decreased thermal stratification. Prandtl number effects were negligible for the two fluids used in this study, water ($Pr \approx 5$) and FC-77 ($Pr \approx 25$). The effect of heater location and spacing was studied by powering various combinations of one or two heater rows. With only one row powered, the average Nusselt number was highest (lowest) when the individual row was located near the cavity floor (ceiling). With two rows energized concurrently, the average Nusselt number, based on a local length scale extending from 6.4 mm below the lowest energized row to the center of each row, increased slightly with decreasing element distance from the bottom wall and increasing row spacing.

A 3 × 3 array of protruding heat sources mounted to one vertical wall has also been considered by Kelleher and coworkers. However, unlike previous studies, the enclosure involved horizontal cold plates and an adiabatic wall opposing the vertical heat source array. A three-dimensional, time-dependent numerical simulation was performed by Liu et al. (1987), with isothermal conditions maintained at both horizontal boundaries. They concluded that the temperature field in the enclosure was characterized by boundary layer-type behavior in regions sur-

[1] Current address: Institute of Paper Science and Technology, 500 10th Street N.W., Atlanta, GA 30318-5794.

Contributed by the Heat Transfer Division for publication in the JOURNAL OF HEAT TRANSFER. Manuscript received by the Heat Transfer Division December 1994; revision received July 1995. Keywords: Electronic Equipment, Enclosure Flows, Natural Convection. Associate Technical Editor: J. R. Lloyd.

rounding the individual heaters and stable stratification elsewhere. A similar arrangement was experimentally studied by Joshi et al. (1990). As the power dissipation from each component was incrementally increased from 0.1 to 3.1 W, three-dimensional flow of increasing complexity was observed. In an extension of this study, Joshi et al. (1991) determined that heat transfer increased by 15 to 20 percent with increasing enclosure width, indicating that the surface area of the horizontal cold plate had an important influence on the outcome of their experiment. This geometry was also numerically modeled by Mukutmoni et al. (1993).

The current study numerically examines three-dimensional natural convection from a 3 × 3 array of heat sources flush-mounted to one vertical wall of a rectangular cavity, with the opposing wall isothermally cooled. Square heat sources ($A_{htr} = 1.0$) are initially simulated by the three-dimensional model, and results are compared to those obtained from a two-dimensional approximation. The heater aspect ratio is then varied to determine conditions for which a two-dimensional approximation is valid. In a companion paper (Heindel et al., 1995a), predictions are compared with experimental results.

This study ignores conductive spreading through the substrate (conjugate heat transfer). Three-dimensional calculations have been performed for a similar geometry in which conjugate effects were included (Heindel et al., 1995b). These predictions revealed that as the substrate/fluid thermal conductivity ratio increased to 4.7, heater edge effects were smoothed out by substrate conduction and two-dimensional flow conditions were approached.

Numerical Model

Figure 1 displays a schematic of the simulated geometry and summarizes the fixed geometric parameters. This geometry is identical to that described in the companion paper (Heindel et al., 1995a), where one vertical wall is composed of a 3 × 3 array of discrete, flush-mounted, isoflux heat sources, with the remainder of the wall being adiabatic. The opposite wall is maintained isothermal and the remaining walls are assumed adiabatic. Since symmetry was observed in previous fully three-dimensional calculations (Fusegi et al., 1991; Wroblewski and Joshi, 1992, 1994) and experimentally confirmed by Ozoe et al. (1979), Hiller et al. (1989), and Heindel (1994), a plane of symmetry at $x = D/2$ ($X = D/(2L_z)$) is used to reduce the computational domain by a factor of two.

Governing Equations. The nondimensional governing equations for three-dimensional laminar natural convection in a discretely heated cavity, assuming constant properties and the Boussinesq approximation, are as follows:

Continuity:

$$\frac{\partial U}{\partial X} + \frac{\partial V}{\partial Y} + \frac{\partial W}{\partial Z} = 0 \tag{1}$$

Momentum:

$$U\frac{\partial U}{\partial X} + V\frac{\partial U}{\partial Y} + W\frac{\partial U}{\partial Z} = \mathrm{Pr}\left[\frac{\partial^2 U}{\partial X^2} + \frac{\partial^2 U}{\partial Y^2} + \frac{\partial^2 U}{\partial Z^2}\right] - \frac{\partial P}{\partial X} \tag{2}$$

$$U\frac{\partial V}{\partial X} + V\frac{\partial V}{\partial Y} + W\frac{\partial V}{\partial Z} = \mathrm{Pr}\left[\frac{\partial^2 V}{\partial X^2} + \frac{\partial^2 V}{\partial Y^2} + \frac{\partial^2 V}{\partial Z^2}\right] - \frac{\partial P}{\partial Y} \tag{3}$$

$$U\frac{\partial W}{\partial X} + V\frac{\partial W}{\partial Y} + W\frac{\partial W}{\partial Z} = \mathrm{Pr}\left[\frac{\partial^2 W}{\partial X^2} + \frac{\partial^2 W}{\partial Y^2} + \frac{\partial^2 W}{\partial Z^2}\right] - \frac{\partial P}{\partial Z} + \mathrm{Ra}^*_{L_z}\,\mathrm{Pr}\,\theta \tag{4}$$

Energy:

$$U\frac{\partial \theta}{\partial X} + V\frac{\partial \theta}{\partial Y} + W\frac{\partial \theta}{\partial Z} = \frac{\partial^2 \theta}{\partial X^2} + \frac{\partial^2 \theta}{\partial Y^2} + \frac{\partial^2 \theta}{\partial Z^2} \tag{5}$$

where the modified Rayleigh number is based on the heater length and the isoflux condition applied at the heater. The nondimensional parameters are defined in the nomenclature. The governing equations reduce to those describing the two-dimensional model when $U = \partial/\partial X = \partial^2/\partial X^2 = 0$.

The boundary conditions at the enclosure walls and the plane of symmetry are:

- At $X = 0$: $U = V = W = 0$ (6)

$$\frac{\partial \theta}{\partial X} = 0 \tag{7}$$

- At $X = \dfrac{D}{2L_z}$: $U = \dfrac{\partial V}{\partial X} = \dfrac{\partial W}{\partial X} = 0$ (8)

$$\frac{\partial \theta}{\partial X} = 0 \tag{9}$$

Nomenclature

A_h = heater wetted surface area = $L_x L_z$
A_{htr} = heater aspect ratio = L_x/L_z
A_x = cavity minor aspect ratio = D/S
A_z = cavity major aspect ratio = H/S
D = cavity depth
g = gravitational acceleration
H = cavity height
k = thermal conductivity
L_x = heater length in the spanwise (x) direction
L_z = heater length in the vertical (z) direction
Nu_{L_z} = local Nusselt number, Eq. (16)
$\overline{\mathrm{Nu}}_{L_z}$ = average Nusselt number, Eq. (17)
P = dimensionless pressure = $p_d/(\rho(\alpha/L_z)^2)$
Pr = Prandtl number = ν/α
P_x = heater pitch in the spanwise (x) direction
P_z = heater pitch in the vertical (z) direction
p_d = dynamic pressure
q'' = applied heat flux
$\mathrm{Ra}^*_{L_z}$ = modified Rayleigh number = $g\beta q'' L_z^4/(k\alpha\nu)$
S = cavity width
T = temperature
U, V, W = dimensionless velocity components, e.g., uL_z/α
u, v, w = velocity components
X, Y, Z = dimensionless coordinates, e.g., x/L_z
x, y, z = coordinate directions
α = thermal diffusivity
β = volumetric thermal expansion coefficient
θ = dimensionless temperature = $(T - T_c)/(q''L_z/k)$
λ_i = cavity heater locations (Fig. 1)
ν = kinematic viscosity
ρ = fluid density

Subscripts

c = cold plate
(i, j) = heater (i, j)
Ri = row i

Superscripts

$\bar{}$ = average

- At $Y = 0$: $U = V = W = 0$ (10)

$$\frac{\partial \theta}{\partial Y} = \begin{cases} 0 & \text{(adiabatic region)} \\ -1 & \text{(isoflux region)} \end{cases} \quad (11)$$

- At $Y = \frac{S}{L_z}$: $U = V = W = 0$ (12)

$$\theta = 0 \quad (13)$$

- At $Z = 0$ and $Z = \frac{H}{L_z}$: $U = V = W = 0$ (14)

$$\frac{\partial \theta}{\partial Z} = 0 \quad (15)$$

Local and average Nusselt numbers are obtained from the resulting temperature field and defined as

$$\mathrm{Nu}_{L_z}(x, z) = \frac{q'' L_z}{(T(x, z)|_{y=0} - T_c)k} = \frac{1}{\theta|_{Y=0}} \quad (16)$$

$$\overline{\mathrm{Nu}}_{L_z,(i,j)} = \frac{q'' L_z}{k} \frac{1}{\frac{1}{A_h}\int_{A_h} (T(x, z)|_{y=0} - T_c) dA_h}$$

$$= \frac{1}{\frac{1}{A_h}\int_{A_h} \theta|_{Y=0} dA_h} \quad (17)$$

where q'' is the applied heat flux, $T(x, z)|_{y=0}$ is the local heater surface temperature, and A_h is the heater area. The subscript (i, j) refers to a specified heater (i, j) in row i and column j. For example, heater (1, 2) is indicated in Fig. 1. Using L_z as the characteristic length in the local and average Nusselt number simplifies the definition and facilitates subsequent comparisons between averaged experimental and numerical values (Heindel et al., 1995a).

Solution Procedure. The governing partial differential equations were discretized on a nonuniform, 30 × 30 × 68 ($X \times Y \times Z$) grid using a control-volume formulation. Control volumes were clustered near wall regions and near regions of discontinuity in the thermal boundary condition. The finite-differencing procedure ensured conservation of mass, momentum, and energy over each control volume. Velocity control volumes were staggered with respect to the main control volumes, and coupling of the pressure and velocity fields was treated via the SIMPLER algorithm (Patankar, 1980). Combined convective and diffusive fluxes across the control surfaces were modeled using the power-law scheme. The resulting algebraic equations were then iteratively solved using a line-by-line TDMA solution procedure.

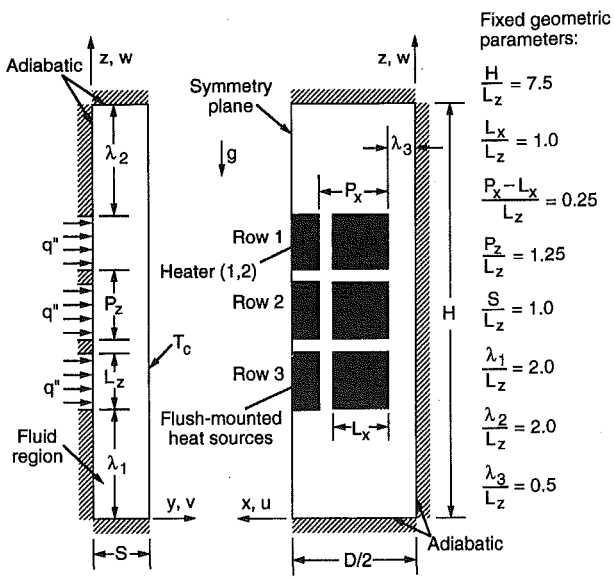

Fig. 1 Discretely heated cavity geometry

The overall solution algorithm used in this study involved initially obtaining a two-dimensional solution at a modified Rayleigh number for which heat transfer is conduction dominated ($\mathrm{Ra}^*_{L_z} = 10^4$). This solution was then used as input to the calculations at the next higher modified Rayleigh number. This process continued until $\mathrm{Ra}^*_{L_z} = 10^8$. Steady-state solutions were obtained at each modified Rayleigh number using underrelaxation techniques. Only the momentum equations were underrelaxed by a relaxation factor of 0.85 for the initial solution. As the modified Rayleigh number was increased, the momentum equation relaxation factors were slowly decreased. Underrelaxation of the energy equation was also used at higher modified Rayleigh numbers, with relaxation factors typically on the order of 0.95. For $A_{\mathrm{htr}} = 1.0$, solutions from the two-dimensional calculations were used as input at all X-plane locations for the three-dimensional calculations, with $U(x, y, z)$ initialized to zero throughout the entire computational domain. Prior three-dimensional calculations were then used as initial conditions in the parametric study of heater aspect ratio effects. The U momentum equation was also underrelaxed in the three-dimensional calculations, but did not require as much underrelaxation as the other momentum equations.

Solutions were considered converged at each test condition after two criteria were satisfied. First, the ratio of residual mass source to the maximum mass flux across a control surface was required to be below 10^{-3}. Second, the iteration-to-iteration change was examined at every nodal location for all calculated values. However, to reduce the likelihood of false convergence related to small but persistent changes between successive iterations due to underrelaxation, the examinations were implemented between iterations I and I-20. The change in computed value, when compared to the maximum value in the domain, was required to be less than 0.5 percent for a solution to be considered converged. This comparison method did not eliminate the possibility of false convergence, but it did reduce it. Typically, the second criterion was the last to be satisfied.

The numerical code and procedure were validated (Heindel, 1994) by obtaining excellent agreement with the benchmark results for natural convection in differentially heated two-dimensional (de Vahl Davis, 1983) and three-dimensional (Fusegi et al., 1991) cavities.

In view of the sizable computational effort involved in the three-dimensional calculations, only a partial grid-independence study was performed (Heindel, 1994). This study focused on the two-dimensional approximation of the cavity with the highest modified Rayleigh number ($\mathrm{Ra}^*_{L_z} = 10^8$) to ensure that the thinnest velocity and thermal boundary layers were satisfactorily resolved. By increasing the grid size from 30 × 68 ($Y \times Z$) to 40 × 96, the average heat transfer rate and stream function changed by less than 2 percent, revealing that the 30 × 68 grid was sufficient to resolve the Y–Z velocity and temperature fields. The grid deployment scheme used over the heater array in the Z direction was then used over the heater array in the X direction for the three-dimensional calculations.

Results

Comparisons Between Two- and Three-Dimensional Calculations. To assess the validity of a two-dimensional approx-

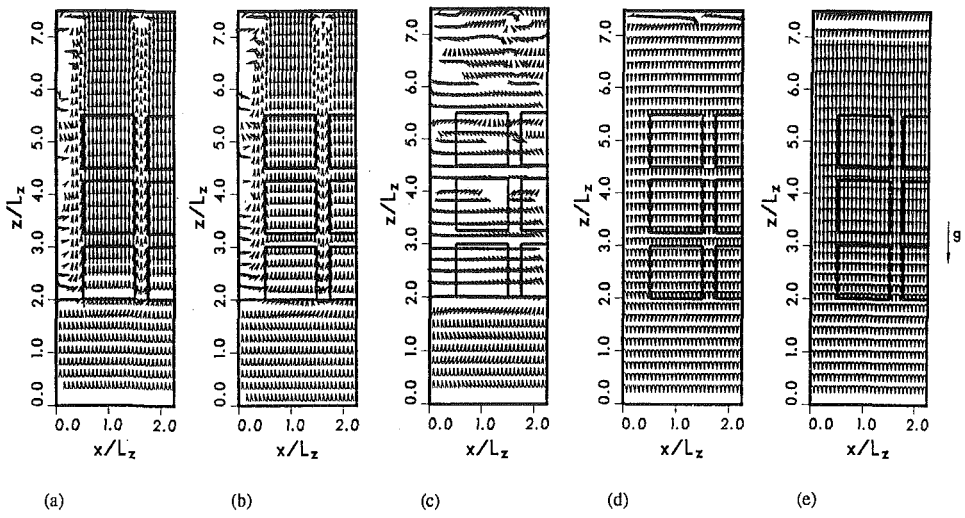

Fig. 2 Velocity vectors at selected y/L_z locations for $Ra^*_{L_z} = 10^8$, Pr = 5.0, A_z = 7.5, and A_{htr} = 1.0: (*a*) y/L_z = 0.05, (*b*) y/L_z = 0.1, (*c*) y/L_z = 0.5, (*d*) y/L_z = 0.9, (*e*) y/L_z = 0.95

imation to a 3 × 3 array of square (A_{htr} = 1.0) discrete heat sources, two-dimensional calculations were performed under the assumption that the heater columns merged to form a single column of strip heaters. Hence, $L_x = D$ and the 3 × 3 array of discrete heat sources in the three-dimensional model is reduced to a 3 × 1 array of strip heat sources for the two-dimensional approximation. The two and three-dimensional calculations encompass a modified Rayleigh number range of $10^5 \leq Ra^*_{L_z} \leq 10^8$ for a fixed Prandtl number and cavity aspect ratio of 5 and 7.5, respectively.

The three dimensionality of the flow can be qualitatively represented by velocity vector plots at various X–Z planes as shown in Fig. 2 for $Ra^*_{L_z} = 10^8$. Although all calculations were performed on a nonuniform grid, the vector plots have been interpolated onto a uniform grid for presentation purposes. All vectors are scaled relative to the maximum value within the entire three-dimensional domain, which is assigned a length of $L_z/2$. Vector magnitudes less than 0.1 percent of the maximum magnitude are not plotted to show regions of relatively stagnant flow. The solid rectangles in each vector plot indicate locations of the discrete heat sources at $y/L_z = 0$.

Two-dimensional flow would exist if all of the velocity vectors were vertical lines. Clearly, such is not the case. Figure 2(*a*) displays the X–Z velocity vectors near the heated wall (y/L_z = 0.05) and close to the maximum vertical velocity for $Ra^*_{L_z} = 10^8$ (see Fig. 3). The upward motion of fluid below row 3 is balanced by regions of downflow at other y locations (e.g., Fig. 2*e*). Fluid acceleration near the heated regions entrains a small amount of fluid from the X direction, which is visible at the heater corners in row 3. Moving up the heated wall, the fluid continues to accelerate and the primary flow is in the vertical direction, with the maximum velocity near the heater midlines and local minima between the heater columns. The almost vertical orientation of the vectors indicates minimal fluid entrainment from the X direction. On approaching the cavity ceiling, the rising plume begins to decelerate and turns toward the cold plate (perpendicular to the figure). Some of the fluid also bifurcates upon impingement with the ceiling, but this fluid is eventually swept toward the cold plate by the bulk fluid motion, forming counterrotating, helical cells.

At y/L_z = 0.1 (Fig. 2*b*), the rising fluid velocity diminishes near the heater surfaces because this plane is near the outer region of the velocity boundary layer (again, see Fig. 3). At the Y midplane (Fig. 2*c*), the vertical velocity diminishes considerably and the dominant flow direction is perpendicular to the figure. The W and U velocities in this region are of the same order of magnitude, and complex flow patterns develop. However, these velocities are very small, compared to the maximum velocities in the cavity, and some regions are nearly stagnant. The helical flow pattern caused by the bifurcating plumes is still visible at the cavity ceiling.

On approaching the cold plate at y/L_z = 0.9 (Fig. 2*d*), the majority of the fluid motion is downward and very uniform. Remnants of the complex helical flow pattern are still apparent at the top of the cavity. Very near the cold plate (Fig. 2*e*), all of the fluid is descending in a uniform fashion. The velocity quickly increases from zero at the cavity ceiling to a nearly constant value in the upper regions of the cavity. Near z/L_z = 3.0, the magnitude of the descending velocity begins to decrease with only small velocities existing in the lower cavity regions.

To compare the predicted three-dimensional velocity profiles to those generated by the two-dimensional model, selected X-

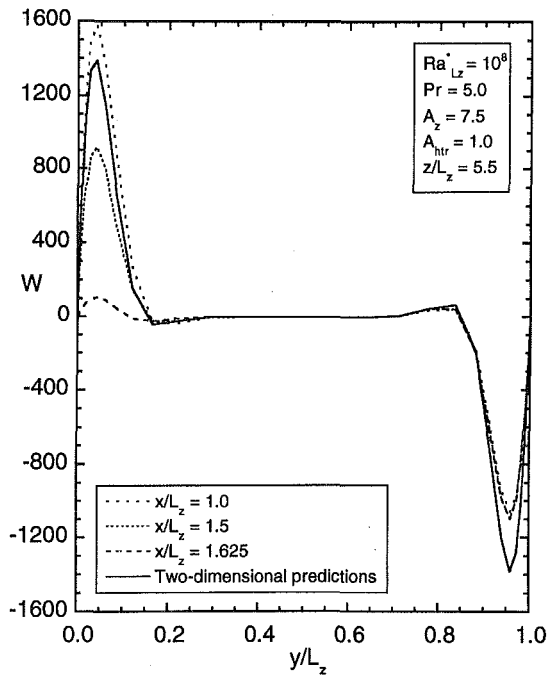

Fig. 3 W velocity profiles at z/L_z = 5.5 and selected x/L_z locations for $Ra^*_{L_z} = 10^8$, Pr = 5.0, A_z = 7.5, and A_{htr} = 1.0

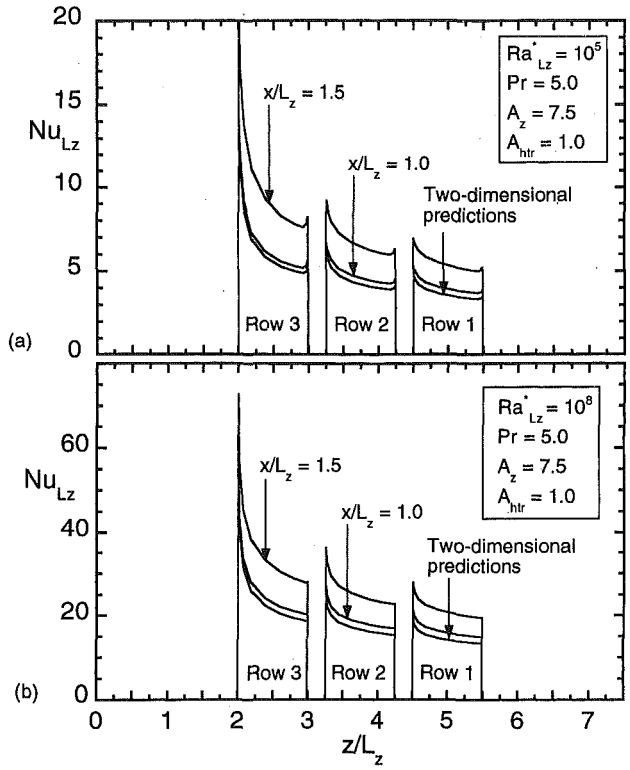

Fig. 4 Local Nusselt number profiles at selected x/L_z locations for Pr = 5.0, A_z = 7.5, and A_{htr} = 1.0: (*a*) $Ra^*_{L_z} = 10^5$, (*b*) $Ra^*_{L_z} = 10^8$

location slices are taken at the midline of heater column 1 ($x/L_z = 1.0$), the edge of heater column 1 ($x/L_z = 1.5$), and the midline of the adiabatic region between heater columns 1 and 2 ($x/L_z = 1.625$). Figure 3 displays the vertical velocity profiles at these locations, as well as the vertical velocity profile predicted by the two-dimensional model, for $Ra^*_{L_z} = 10^8$ and $z/L_z = 5.5$. Near the hot wall ($y/L_z = 0$), the heater midline predictions exceed the two-dimensional predictions. This behavior is due to the small amount of lateral fluid entrainment near the heater edges. From continuity considerations, this effect increases the vertical velocity at the heater midline over that predicted by the two-dimensional model. The vertical velocities at $x/L_z = 1.5$ and 1.625 are smaller than those predicted by the two-dimensional model because the adiabatic region between heater columns reduces the local buoyant force. The boundary layer thicknesses predicted by both models are nearly identical, as is the extent of the stagnant core region.

Near the cold plate ($y/L_z \approx 1.0$), all three velocity profiles at the selected X locations collapse to one curve, signifying uniform flow across the cold plate. Velocities predicted by the three-dimensional model are smaller than those predicted by the two-dimensional model because the overall flow rate per unit depth from the heated wall to the cold plate is smaller in the three-dimensional model due to nonuniform heating of the fluid in the depth (X) direction.

Major differences in heat transfer are associated with the two and three-dimensional model predictions. The local Nusselt number distributions predicted by the three-dimensional model at the midline and edge of heater column 1 ($x/L_z = 1.0$ and 1.5, respectively) are compared with the two-dimensional predictions in Fig. 4(a) for $Ra^*_{L_z} = 10^5$. For row 3, both models reveal a decrease in the local Nusselt number from a maximum at the leading edge ($z/L_z = 2.0$) to the trailing edge ($z/L_z = 3.0$). However, both models also predict a slight enhancement in the local Nusselt number at the trailing edge, which is caused by streamwise diffusion to the relatively cool fluid in the adiabatic region beyond the trailing edge. Similar distributions are predicted for the downstream heaters, with a slight increase over the value at the trailing edge of the upstream heater characterizing conditions at the leading edge of rows 1 and 2. This increase is due to partial dissipation of the thermal boundary layer in the adiabatic region between heaters and renewal of thermal boundary layer development at the leading edge of the downstream heater.

The largest Nusselt numbers are associated with the edge ($x/L_z = 1.5$) of heater column 1, and differences relative to the other distributions are attributed to two factors: lateral entrainment of relatively cool fluid from the adjacent adiabatic regions and diffusion from warm fluid flowing over the heater surface to cool fluid in the adiabatic region. Both effects increase the local heat transfer at the heater edge. Additionally, three-dimensional predictions at the heater midline ($x/L_z = 1.0$) are about 5 percent higher than the two-dimensional results due to the larger midline velocities predicted by the three-dimensional model.

Increasing the modified Rayleigh number to 10^8 (Fig. 4b) increases the local Nusselt number over all heated regions, and similar trends are obtained. However, the significance of streamwise diffusion at the trailing edge of each heat source diminishes, relative to the increased convection coefficient, and local enhancement of heat transfer at the trailing edge is negligible.

As shown in Fig. 5, edge effects predicted by the three-dimensional model significantly influence the row-averaged Nusselt number ($\overline{Nu}_{L_z,Ri}$) and dimensionless average surface temperature ($\overline{\theta}_{Ri}$). Although actual temperatures increase with increasing heat flux, the increase in $T - T_c$ is not commensurate with the increase in q'' and $\overline{\theta}_{Ri}$ decreases with increasing $Ra^*_{L_z}$. Each model predicts the highest row-averaged Nusselt number and the lowest dimensionless surface temperature for row 3 because the thermal boundary layer is thinnest and the local bulk fluid temperature is lowest in this region. The row-averaged Nusselt number is lowest for row 1 because of a relatively thick thermal boundary layer and a high local bulk fluid temperature. Predictions of $\overline{Nu}_{L_z,Ri}$, based on the three-

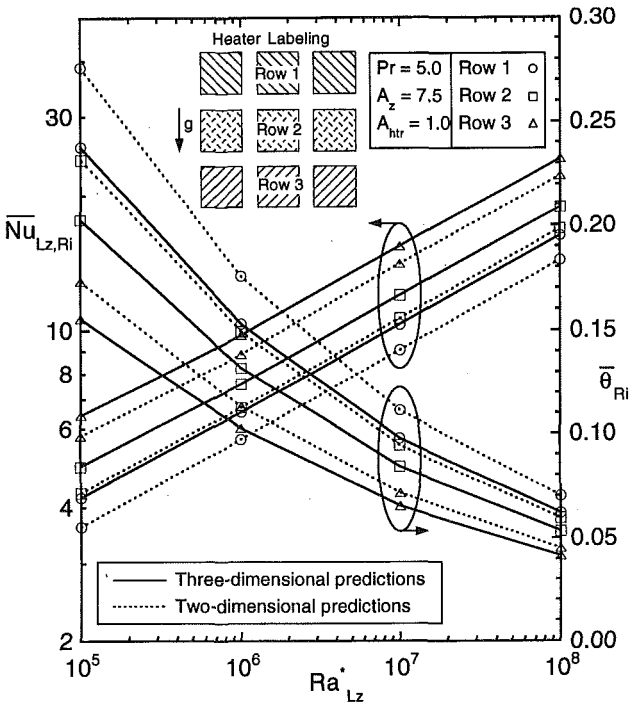

Fig. 5 Comparisons of two and three-dimensional predictions of the row-averaged Nusselt number and dimensionless surface temperature for Pr = 5.0, A_z = 7.5, and A_{htr} = 1.0

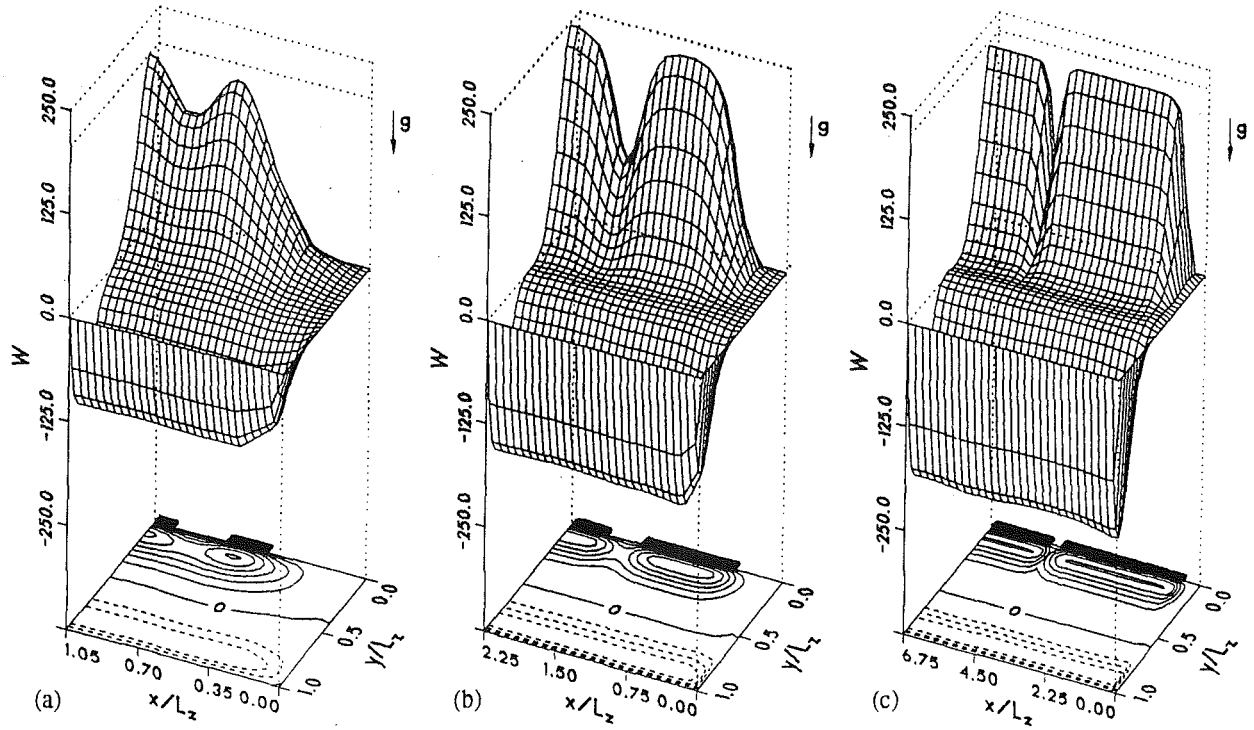

Fig. 6 Effect of heater aspect ratio on the spanwise (X) distribution of the vertical velocity component at $z/L_z = 5.5$ for $Ra^*_{L_z} = 10^6$, Pr = 5.0, and $A_z = 7.5$: (*a*) $A_{htr} = 0.2$, (*b*) $A_{htr} = 1.0$, (*c*) $A_{htr} = 4.0$. Note the scale changes in the x/L_z direction

dimensional model, are 10 to 15 percent higher than those of the two-dimensional model, and the differences are attributed solely to lateral edge effects captured by the three-dimensional model. This trend is also manifested by the reduced average heater surface temperatures predicted by the three-dimensional model.

Effect of Heater Aspect Ratio. The effect of heater aspect ratio ($A_{htr} = L_x/L_z$) on fluid flow and heat transfer within a discretely heated cavity was studied by fixing the modified Rayleigh number at 10^6. The Prandtl number and cavity major aspect ratio also remained fixed at 5.0 and 7.5, respectively. The heater aspect ratio was varied between 0.2 and 4.0 by changing the heater width in the X direction (L_x). The width of the adiabatic region between heater columns was fixed at its original value of 0.25 L_z. Therefore, the heater pitch in the X direction varied from 0.45 to 4.25.

The effect of heater aspect ratio on the vertical velocity profile is shown in Fig. 6 for conditions at the trailing edge of row 1 ($z/L_z = 5.5$). The darkened regions along $y/L_z = 0$ signify the locations of the heater columns. Because the scale along the X coordinate changes between figures, the physical length of the adiabatic region between columns appears to decrease as A_{htr} increases, even though it remains the same. This figure shows that as A_{htr} increases, the vertical velocity profile across the heater face (in the X direction) becomes more uniform. Differences between the maximum velocity and the local minimum in the adiabatic region between heater columns also increase with increasing A_{htr}.

The foregoing trends may be explained via fluid drag and continuity considerations. At $A_{htr} = 0.2$, the horizontal width of the heater is not sufficient to provide a buoyant force strong enough to completely overcome the drag induced by the cooler adjacent fluid regions. Hence, the velocity profile does not completely develop, as indicated by the lack of uniformity near the heater midline. For $A_{htr} = 1.0$, enough fluid is heated to overcome the drag of the cooler fluid in the adjacent adiabatic regions. The X distribution of the vertical velocity component is well developed at the heater midline, and due to lateral fluid entrainment and continuity, the velocity is higher than that predicted by the two-dimensional model (Fig. 7). For $A_{htr} = 4.0$, the vertical velocity is uniform over a wide range of X, indicating nearly two-dimensional conditions. Lateral fluid entrainment at the heater edges is insignificant compared to the bulk

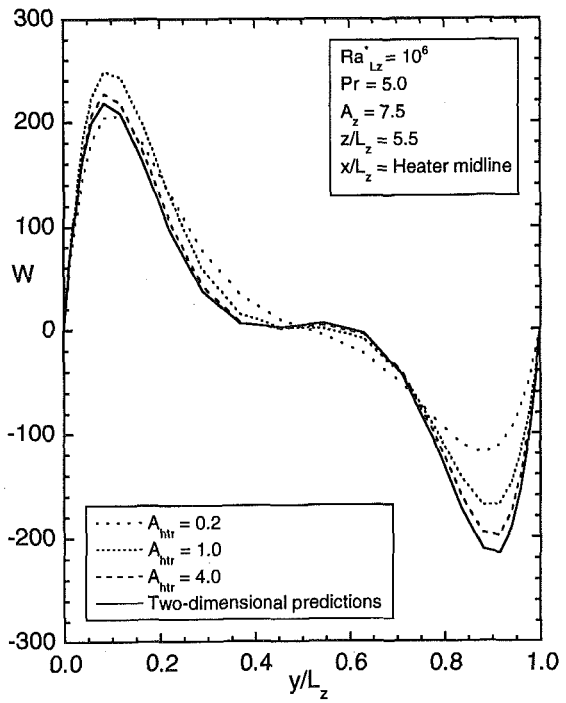

Fig. 7 Effect of heater aspect ratio on the variation of the vertical velocity component at $z/L_z = 5.5$ and the heater midline of column 2 for $Ra^*_{L_z} = 10^6$, Pr = 5.0, and $A_z = 7.5$

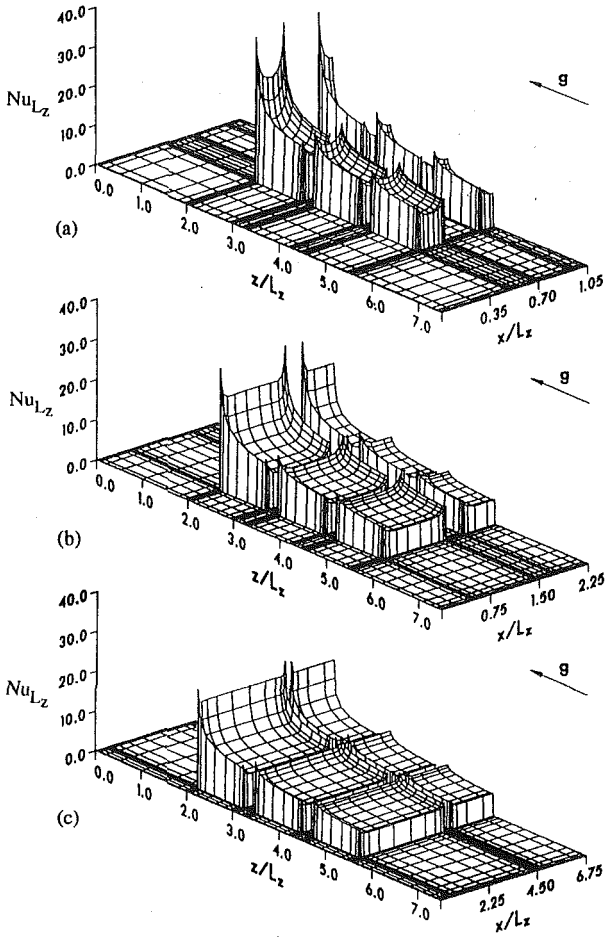

Fig. 8 Effect of heater aspect ratio on the local Nusselt number distribution for $Ra^*_{L_z} = 10^6$, Pr = 5.0, and $A_z = 7.5$: (*a*) $A_{htr} = 0.2$, (*b*) $A_{htr} = 1.0$, (*c*) $A_{htr} = 4.0$. Note the orientation of the gravity vector.

fluid motion and does not increase the maximum velocity much above that predicted by the two-dimensional model.

The effect of A_{htr} on the maximum vertical velocity at the heater midplane of column 2 is also shown by plotting vertical velocity profiles in this plane for different A_{htr} (Fig. 7). Along the heated wall ($y/L_z \approx 0$), velocities are smallest for $A_{htr} = 0.2$ and largest for $A_{htr} = 1.0$. For $A_{htr} = 4.0$, the velocity profile approaches that predicted by the two-dimensional model. Additionally, the magnitude of the descending vertical velocity along the cold plate increases as A_{htr} increases, with that obtained for $A_{htr} = 4.0$ approaching the two-dimensional predictions. As discussed previously, the average mass flow rate associated with the two-dimensional model is higher than that for the three-dimensional model. As A_{htr} increases, each row of heaters approaches the limit of continuous strip heaters. Consequently, the average mass flow rate increases as A_{htr} increases.

The effect of heater aspect ratio on the local Nusselt number is shown in Fig. 8, where increasing A_{htr} influences Nu_{L_z} in three ways: (*i*) The local Nusselt number becomes more uniform across the heater face; (*ii*) the larger heated area diminishes the significance of edge effects, relative to total heat transfer; and (*iii*) the maximum local Nusselt number decreases (note the spikes at the heater corners). The third effect is due to the reduction in the amount of cool fluid in the adiabatic regions, compared to the amount of relatively warm fluid over the heater surface. Hence, the amount by which the maximum value of Nu_{L_z} decreases would likely change if the size of the adiabatic gap between heater columns (and end wall) were allowed to change with varying A_{htr}.

The significance of the edge effects becomes evident when the row-averaged Nusselt number is plotted as a function of A_{htr} (Fig. 9). For $A_{htr} = 0.2$, the three-dimensional predictions are 54, 49, and 36 percent higher than the two-dimensional results for rows 1, 2, and 3, respectively. For $A_{htr} \gtrsim 3.0$, the two- and three-dimensional model predictions are within about 5 percent. Therefore, a designer could use two-dimensional model predictions with confidence when $A_{htr} \gtrsim 3.0$. This result is consistent with predictions by Wroblewski and Joshi (1994), who studied a single heat source mounted in a cubic cavity. Therefore, to maintain the highest possible heat transfer from an electronics component with a rectangular surface area, the longest side should be oriented vertically to maximize edge effects.

Conclusions

Two and three-dimensional laminar natural convection calculations have been performed for a 3 × 3 array of discrete heat sources flush-mounted to one vertical wall of a rectangular cavity whose opposite wall was isothermally cooled. Comparisons between results were made for $10^5 \le Ra^*_{L_z} \le 10^8$, Pr = 5, $A_z = 7.5$, and $0.2 \le A_{htr} \le 4.0$.

Overall, variations between the two and three-dimensional velocity predictions were small and were mainly confined to the adiabatic regions between heater columns. However, the three-dimensional model captured edge effects that could not be predicted by the two-dimensional model. These edge effects, which included local variations in the velocity and temperature fields, did influence local and overall heat transfer rates. Although the local Nusselt number predicted by the three-dimensional model at the heater midplane was only about 5 percent higher than that predicted by the two-dimensional model for $A_{htr} = 1.0$, the three-dimensional model predicted significant enhancement at the lateral edges, which yielded a 10 to 15 percent increase in row-averaged Nusselt numbers. The higher Nusselt numbers predicted by the three-dimensional model correspond to lower surface-averaged temperatures.

With increasing heater aspect ratio, A_{htr}, the vertical velocity component and local Nusselt number became more uniformly

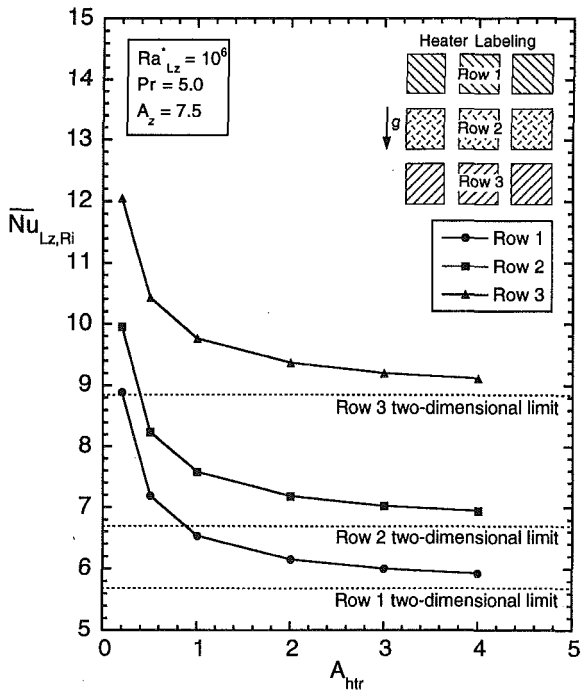

Fig. 9 Effect of heater aspect ratio on the row-averaged Nusselt numbers for $Ra^*_{L_z} = 10^6$, Pr = 5.0, and $A_z = 7.5$

distributed across the heater face. Adjacent to the heated wall, the vertical velocity was highest for $A_{htr} = 1.0$, while the row-averaged Nusselt number was highest for $A_{htr} = 0.2$. Row-averaged Nusselt numbers decreased with increasing A_{htr}. Also, as A_{htr} increased, three-dimensional predictions approached those of the two-dimensional model, with row-averaged Nusselt numbers agreeing to within 5 percent for $A_{htr} \gtrsim 3.0$. Therefore, to obtain accurate heat transfer predictions, a three-dimensional model is only necessary when $A_{htr} \lesssim 3$. If two-dimensional models are used under these conditions, heat transfer rates would be underestimated.

Acknowledgments

Support of this work by the National Science Foundation under Grant No. CTS-9004213 is gratefully acknowledged.

References

Bar-Cohen, A., 1992, "State-of-the-Art and Trends in the Thermal Packaging of Electronic Equipment," ASME *Journal of Electronic Packaging,* Vol. 114, pp. 257–270.

Bar-Cohen, A., 1993, "Thermal Management of Electronic Components With Dielectric Liquids," *JSME International Journal, Series B,* Vol. 36, pp. 1–25.

de Vahl Davis, G., 1983, "Natural Convection of Air in a Square Cavity: A Bench Mark Numerical Solution," *International Journal for Numerical Methods in Fluids,* Vol. 3, pp. 249–264.

Fusegi, T., Hyun, J. M., Kuwahara, K., and Farouk, B., 1991, "A Numerical Study of Three-Dimensional Natural Convection in a Differentially Heated Cubical Enclosure," *International Journal of Heat and Mass Transfer,* Vol. 34, pp. 1543–1557.

Heindel, T. J., 1994, "A Numerical and Experimental Study of Three-Dimensional Natural Convection in a Discretely Heated Cavity," Ph.D. Thesis, Purdue University, West Lafayette, IN.

Heindel, T. J., Incropera, F. P., and Ramadhyani, S., 1995a, "Laminar Natural Convection in a Discretely Heated Cavity: II—Comparisons of Experimental and Theoretical Results," ASME JOURNAL OF HEAT TRANSFER, Vol. 117, this issue, pp. 910–917.

Heindel, T. J., Ramadhyani, S., and Incropera, F. P., 1995b, "Conjugate Natural Convection From an Array of Discrete Heat Sources: Part 1—Two- and Three-Dimensional Model Validation," *International Journal of Heat and Fluid Flow,* in press.

Hiller, W. J., Koch, S., and Kowalewski, T. A., 1989, "Three-Dimensional Structures in Laminar Natural Convection in a Cubic Enclosure," *Experimental Thermal and Fluid Science,* Vol. 2, pp. 34–44.

Incropera, F. P., 1988, "Convection Heat Transfer in Electronic Equipment Cooling," ASME JOURNAL OF HEAT TRANSFER, Vol. 110, pp. 1097–1111.

Jaluria, Y., 1985, "Natural Convective Cooling of Electronic Equipment," *Natural Convection Fundamentals and Applications,* S. Kakac, W. Aung, and R. Viskanta, eds., Hemisphere Publishing Corp., pp. 961–986.

Joshi, Y., Kelleher, M. D., and Benedict, T. J., 1990, "Natural Convection Immersion Cooling of an Array of Simulated Electronic Components in an Enclosure Filled With Dielectric Fluid," *Heat Transfer in Electronic and Microelectronic Equipment—1990,* A. E. Bergles, ed., Hemisphere, New York, pp. 445–468.

Joshi, Y., Kelleher, M. D., Powell, M., and Torres, E. I., 1991, "Natural Convection Heat Transfer From an Array of Rectangular Protrusions in an Enclosure Filled With Dielectric Liquid," *Heat Transfer Enhancement in Electronics Cooling,* ASME HTD-Vol. 183, S. H. Bhavnani and M. Greiner, eds., pp. 9–18.

Kuhn, D., and Oosthuizen, P. H., 1986, "Three-Dimensional Transient Natural Convective Flow in a Rectangular Enclosure With Localized Heating," *Natural Convection in Enclosures—1986,* ASME HTD-Vol. 63, R. S. Figliola and I. Catton, eds., pp. 55–62.

Liu, K. V., Yang, K. T., and Kelleher, M. D., 1987, "Three-Dimensional Natural Convection Cooling of an Array of Heated Protrusions in an Enclosure Filled With a Dielectric Fluid," *Proceedings of the International Symposium on Cooling Technology for Electronic Equipment,* Honolulu, HI, pp. 486–497.

Mukutmoni, D., Joshi, Y. K., and Kelleher, M. D., 1993, "Computations for a Three-by-Three Array of Protrusions Cooled by Liquid Immersion: Effect of Enclosure Width," *Solutions to CFD Benchmark Problems in Electronic Packaging,* ASME HTD-Vol. 255, D. Agonafer, ed., pp. 45–56.

Ozoe, H., Sato, N., and Churchill, S., 1979, "Experimental Confirmation of the Three-Dimensional Helical Streaklines Previously Computed for Natural Convection in Inclined Rectangular Enclosures," *International Chemical Engineering,* Vol. 19, pp. 454–462.

Patankar, S. V., 1980, *Numerical Heat Transfer and Fluid Flow,* Hemisphere Publishing Corp., New York.

Peterson, G. P., and Ortega, A., 1990, "Thermal Control of Electronic Equipment and Devices," *Advances in Heat Transfer,* Vol. 20, J. P. Hartnett and T. F. Irvine, Jr., eds., pp. 181–314.

Polentini, M. S., Ramadhyani, S., and Incropera, F. P., 1993, "Single-Phase Thermosyphon Cooling of an Array of Discrete Heat Sources in a Rectangular Cavity," *International Journal of Heat and Mass Transfer,* Vol. 36, pp. 3983–3996.

Wroblewski, D., and Joshi, Y., 1992, "Transient Natural Convection From a Leadless Chip Carrier in a Liquid Filled Enclosure: A Numerical Study," *Advances in Electronic Packaging*—1992, EEP-Vol. 1-1, W. T. Chen and H. Abé, eds., pp. 235–248.

Wroblewski, D. E., and Joshi, Y., 1994, "Liquid Immersion Cooling of a Substrate-Mounted Protrusion in a Three-Dimensional Enclosure: The Effects of Geometry and Boundary Conditions," ASME JOURNAL OF HEAT TRANSFER, Vol. 116, pp. 112–119.